Article

Insights into the Mobility of Methyl-Bearing Side Chains in Proteins from *J* and *J* Couplings

James J. Chou, David A. Case, and Ad Bax

J. Am. Chem. Soc., **2003**, 125 (29), 8959-8966• DOI: 10.1021/ja029972s • Publication Date (Web): 26 June 2003

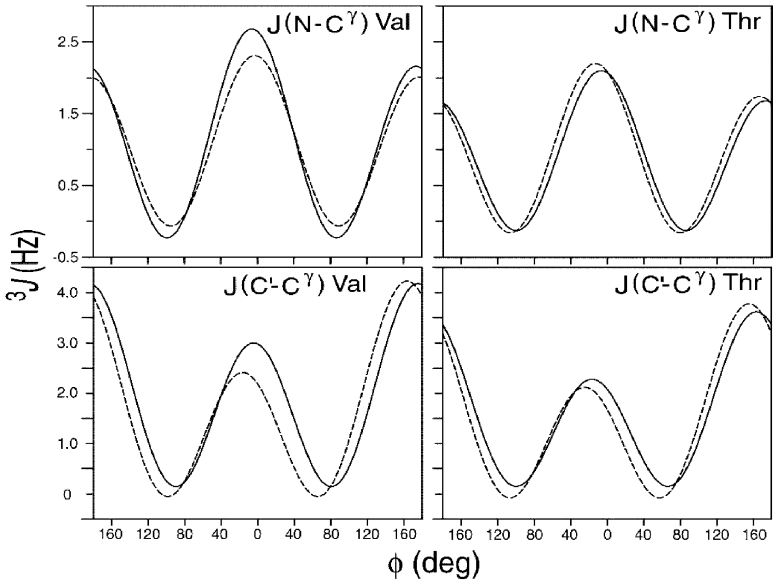

More About This Article

Additional resources and features associated with this article are available within the HTML version:

- Supporting Information
- Links to the 15 articles that cite this article, as of the time of this article download
- Access to high resolution figures
- Links to articles and content related to this article
- Copyright permission to reproduce figures and/or text from this article

View the Full Text HTML

J|A|C|S
ARTICLES
Published on Web 06/26/2003

Insights into the Mobility of Methyl-Bearing Side Chains in Proteins from $^3J_{CC}$ and $^3J_{CN}$ Couplings

James J. Chou,[†,§] David A. Case,[‡] and Ad Bax*[,†]

Contribution from the Laboratory of Chemical Physics, National Institute of Diabetes and Digestive and Kidney Diseases, National Institutes of Health, Bethesda, Maryland 20892, and Department of Molecular Biology, The Scripps Research Institute, La Jolla, California 92037

Received December 31, 2002; E-mail: bax@nih.gov

Abstract: Side-chain dynamics in proteins can be characterized by the NMR measurement of ^{13}C and ^2H relaxation rates. Evaluation of the corresponding spectral densities limits the slowest motions that can be studied quantitatively to the time scale on which the overall molecular tumbling takes place. A different measure for the degree of side-chain order about the $C^\alpha-C^\beta$ bond (χ_1 angle) can be derived from $^3J_{C'-C\gamma}$ and $^3J_{N-C\gamma}$ couplings. These couplings can be measured at high accuracy, in particular for Thr, Ile, and Val residues. In conjunction with the known backbone structures of ubiquitin and the third IgG-binding domain of protein G, and an extensive set of $^{13}C-^1H$ side-chain dipolar coupling measurements in oriented media, these ^3J couplings were used to parametrize empirical Karplus relationships for $^3J_{C'-C\gamma}$ and $^3J_{N-C\gamma}$. These Karplus curves agree well with results from DFT calculations, including an unusual phase shift, which causes the maximum $^3J_{CC}$ and $^3J_{CN}$ couplings to occur for dihedral angles slightly smaller than 180°, particularly noticeable in Thr residues. The new Karplus curves permit determination of rotamer populations for the χ_1 torsion angles. Similar rotamer populations can be derived from side-chain dipolar couplings. Conversion of these rotamer populations into generalized order parameters, $\boldsymbol{S}_J^2$ and $\boldsymbol{S}_D^2$, provides a view of side-chain dynamics that is complementary to that obtained from ^{13}C and ^2H relaxation. On average, results agree well with literature values for ^2H-relaxation-derived $\boldsymbol{S}_{rel}^2$ values in ubiquitin and HIV protease, but also identify a fraction of residues for which $\boldsymbol{S}_{J,D}^2 < \boldsymbol{S}_{rel}^2$. This indicates that some of the rotameric averaging occurs on a time scale too slow to be observable in traditional relaxation measurements.

Introduction

Modern NMR provides an unprecedented view of both backbone and side-chain dynamics in proteins.[1−6] Such studies are motivated by the intricate interplay between dynamics, structure, and function of proteins. Side chains, in particular, can contribute substantial amounts to the residual configurational entropy and thereby modulate thermodynamic aspects of protein function.[7−10] Protein side-chain conformations are also critical to understanding the mechanism of molecular recognition in cellular signaling pathways. Unlike most protein backbone residues, a majority of the side chains exhibit large amplitude rearrangements in a process often referred to as "rotamer hopping", where a side chain rapidly switches between two or three energetically favorable, staggered rotamers. Quantitative definition of the less populated rotameric states, in addition to identification of the most populated side-chain rotamer, presents a major challenge in structural biology.

Much of the recent NMR work to quantify the contribution of side-chain disorder in terms of thermodynamics has focused on measurement of side-chain order parameters, mostly by means of ^{13}C and ^2H relaxation.[5,9−12] These relaxation rates commonly are interpreted in terms of generalized order parameters, $\boldsymbol{S}^2$,[1,13] which in turn are evaluated in terms of their contribution to the entropy of the system.[9,14,15] Indeed, quantitative knowledge of the dynamic properties of side chains can yield valuable insights in understanding protein−protein interaction. This has been demonstrated, for example, for calmodulin where the methyl group $\boldsymbol{S}^2$ values were used to estimate the change in side-chain entropy as a function of temperature and upon binding to a peptide.[9,10] A considerable increase in the

[†] National Institutes of Health.
[‡] The Scripps Research Institute.
[§] Present address: Harvard Medical School, Department of Biological Chemistry and Molecular Pharmacology, Boston, MA 02115.

(1) Kay, L. E.; Torchia, D. A.; Bax, A. *Biochemistry* **1989**, *28*, 8972−8979.
(2) Wagner, G. *Curr. Opin. Struct. Biol.* **1993**, *3*, 748−754.
(3) Wand, A. J.; Urbauer, J. L.; McEvoy, R. P.; Bieber, R. J. *Biochemistry* **1996**, *35*, 6116−6125.
(4) Foster, M. P.; Wuttke, D. S.; Radhakrishnan, I.; Case, D. A.; Gottesfeld, J. M.; Wright, P. E. *Nat. Struct. Biol.* **1997**, *4*, 605−608.
(5) Yang, D. W.; Mittermaier, A.; Mok, Y. K.; Kay, L. E. *J. Mol. Biol.* **1998**, *276*, 939−954.
(6) Palmer, A. G. *Annu. Rev. Biophys. Biomol. Struct.* **2001**, *30*, 129−155.
(7) Yang, D. W.; Mok, Y. K.; FormanKay, J. D.; Farrow, N. A.; Kay, L. E. *J. Mol. Biol.* **1997**, *272*, 790−804.
(8) Gagne, S. M.; Tsuda, S.; Spyracopoulos, L.; Kay, L. E.; Sykes, B. D. *J. Mol. Biol.* **1998**, *278*, 667−686.
(9) Lee, A. L.; Kinnear, S. A.; Wand, A. J. *Nat. Struct. Biol.* **2000**, *7*, 72−77.
(10) Lee, A. L.; Wand, A. J. *Nature* **2001**, *411*, 501−504.
(11) Nicholsom, L. K.; Kay, L. E.; Baldisseri, D. M.; Arango, J.; Young, P. E.; Bax, A.; Torchia, D. A. *Biochemistry* **1992**, *31*, 5253−5263.
(12) Ishima, R.; Petkova, A. P.; Louis, J. M.; Torchia, D. A. *J. Am. Chem. Soc.* **2001**, *123*, 6164−6171.
(13) Lipari, G.; Szabo, A. *J. Am. Chem. Soc.* **1982**, *104*, 4546−4559.
(14) Li, Z. G.; Raychaudhuri, S.; Wand, A. J. *Protein Sci.* **1996**, *5*, 2647−2650.
(15) Bracken, C.; Carr, P. A.; Cavanagh, J.; Palmer, A. G. *J. Mol. Biol.* **1999**, *285*, 2133−2146.

average methyl S^2 values, that is, a loss in side-chain entropy, was observed for Ca^{2+}-calmodulin when binding to a myosin light chain kinase target fragment.

^2H and ^{13}C relaxation measurements only capture motions taking place on a time scale faster than the overall rotational correlation time of the molecule. A conceptually different approach for characterizing side-chain disorder relies on the measurement of three-bond scalar couplings, such as $^3J_{H\alpha-H\beta}$, $^3J_{N-C\gamma}$, $^3J_{C'-C\gamma}$, and $^3J_{C\alpha-C\delta}$, to establish rotamer distributions.[16−18] This approach does not provide information on the time scale at which such averaging takes place, but includes motions over the entire range, from milliseconds to picoseconds. Such analyses have been used extensively for peptides, where $^3J_{H\alpha-H\beta}$ values are readily measured, but interpretation in terms of staggered χ_1 rotamer populations requires that accurate couplings for the trans and gauche conformations are known.[19−21] In proteins, measurement of $^3J_{H\alpha-H\beta}$ at the required high degree of accuracy can be more challenging, and consequently this approach has been used less in a quantitative manner.

The χ_1-angle-related $^3J_{N-C\gamma}$ and $^3J_{C'-C\gamma}$ couplings of Val, Ile, and Thr residues in proteins can easily be measured at high precision.[22,23] Interpretation of these values in terms of rotamer populations requires that accurately parametrized Karplus relations are available. Previous parametrizations have been based mostly on static torsion angles, extracted from X-ray and NMR structures, or on a self-consistency principle, allowing for rotamer averaging.[24] Here, we take a slightly different approach and use both the known backbone structures and the side-chain dipolar couplings measured for two small proteins, ubiquitin and the third IgG-binding domain of protein G, to derive a set of Karplus parameters that is both self-consistent and in agreement with experimental dipolar coupling data, measured in liquid crystalline media.

Comparison of $C'-C^\alpha$ and $C^\alpha-H^\alpha$ residual dipolar couplings (RDCs) with $C^\beta-H^\beta$ RDCs can frequently identify the predominant χ_1 rotamer directly, without the knowledge of protein backbone structure.[25] On the other hand, when the backbone structure is accurately known, rotamer populations can also be obtained by fitting the three-state jump model to RDCs measured for the side-chain $^1H-^{13}C$ bonds.[26] Here, we use RDCs measured for Val, Ile, and Thr side chains of ubiquitin and the third IgG-binding domain of protein G (GB3) to independently determine the distribution of staggered χ_1 rotamers with twist angles of less than 30°. The ensembles of resulting χ_1 angles are subsequently used in a general fitting routine to parametrize the $^3J_{N-C\gamma}$ and $^3J_{C'-C\gamma}$ Karplus curves that best describe the measured $^3J_{N-C\gamma}$ and $^3J_{C'-C\gamma}$ values. Validation of this approach is obtained from DFT calculations, which yield very similar Karplus curves. In addition, we show improved cross validation, where Karplus parameters derived in this manner exclusively from GB3 data provide a better prediction for ubiquitin couplings than the use of discrete, ideal rotamers.

Rotamer populations derived from $^3J_{N-C\gamma}$ and $^3J_{C'-C\gamma}$ couplings are readily converted into generalized order parameters, S_J^2. Comparison of these S_J^2 values with those previously obtained from ^2H relaxation shows good agreement for the majority of residues investigated in ubiquitin and HIV protease, but also shows a subset of residues for which S_J^2 is considerably smaller than the value derived from ^2H relaxation. For this latter subset, rotamer averaging apparently takes place on a time scale slower than ca. 10 ns.

Experimental Section

For the measurement of scalar couplings, isotropic samples of uniformly $^{13}C/^{15}N$-enriched ubiquitin and the third IgG-binding domain of protein G (GB3) were prepared at concentrations of 2 mM, in 25 mM phosphate buffer, pH 6.5, 75 mM NaCl, 90% H_2O, 10% D_2O. A 0.3 mM (dimer) sample of uniformly $^{15}N/^{13}C$-enriched HIV-protease, complexed with the inhibitor DMP323,[27] was prepared as described previously,[28] in 20 mM phosphate buffer, pH 5.8, 90% H_2O, 10% D_2O. All samples had volumes of 250 μL and were loaded into thin-wall Shigemi microcells (Shigemi Inc., Allison Park, PA).

For the measurement of dipolar couplings, two separate samples of GB3 (0.7 mM) in liquid crystal were prepared. One liquid crystalline sample was based on the nearly neutral poly(ethylene glycol) (PEG) based medium, consisting of 4.3% w/v $C_{12}E_5$/*n*-hexanol in a molar ratio of 0.96:1,[29] in 25 mM phosphate buffer, pH 6.5, 75 mM NaCl, 90% H_2O, 10% D_2O. The same conditions were used for the second sample, but the liquid crystal was formed by 11 mg/mL of negatively charged filamentous phage Pf1 (Asla Labs, http://130.237.129.141).[30] No dipolar couplings could be measured in the HIV protease complex due to the lack of an adequate alignment medium.

All NMR measurements were carried out on Bruker 600 and 800 MHz spectrometers, equipped with triple-resonance, three-axis pulsed field gradient probeheads. Spectra were processed and analyzed with the NMRPipe software package.[31] For ubiquitin, resonance assignments and backbone and side-chain RDCs have been reported previously,[3,32] and ^1H and ^{13}C chemical shifts of HIV-protease were also taken from the literature.[28] Assignments of GB3 were made as part of the present study, using a pair of HC(CO)NH- and C(CO)NH-TOCSY experiments,[33] which correlate the side chain with the known backbone assignments (Ramirez, B., unpublished). Dipolar couplings of the methyl groups, $C^\beta-H^\beta$, and $C^\alpha-H^\alpha$ of GB3 were measured using the *J*-modulated $[^1H-^{13}C]$ CT-HSQC experiment[34] at 800 MHz. Scalar couplings $^3J_{N-C\gamma}$ and $^3J_{C'-C\gamma}$ of ubiquitin, GB3, and HIV-protease were measured at 800 MHz using quantitative *J* correlation experiments.[22,23]

The fitting of protein backbone dipolar couplings to known atomic coordinates was performed by means of singular value decomposition

(16) Dzakula, Z.; Westler, W. M.; Edison, A. S.; Markley, J. L. *J. Am. Chem. Soc.* **1992**, *114*, 6195−6199.
(17) Dzakula, Z.; Edison, A. S.; Westler, W. M.; Markley, J. L. *J. Am. Chem. Soc.* **1992**, *114*, 6200−6207.
(18) Perez, C.; Lohr, F.; Ruterjans, H.; Schmidt, J. M. *J. Am. Chem. Soc.* **2001**, *123*, 7081−7093.
(19) Feeney, J. *Proc. R. Soc. London, Ser. A* **1975**, *345*, 61−69.
(20) Wyssbrod, H. R.; Ballardin, A.; Schwartz, I. L.; Walter, R.; van Binst, G.; Gibbons, W. A.; Agosta, W. C.; Field, F. H.; Cowburn, D. *J. Am. Chem. Soc.* **1977**, *99*, 5273−5276.
(21) Fischman, A. J.; Live, D. H.; Wyssbrod, H. R.; Agosta, W. C.; Cowburn, D. *J. Am. Chem. Soc.* **1980**, *102*, 2533−2539.
(22) Vuister, G. W.; Wang, A. C.; Bax, A. *J. Am. Chem. Soc.* **1993**, *115*, 5334−5335.
(23) Grzesiek, S.; Vuister, G. W.; Bax, A. *J. Biomol. NMR* **1993**, *3*, 487−493.
(24) Schmidt, J. M.; Blumel, M.; Lohr, F.; Ruterjans, H. *J. Biomol. NMR* **1999**, *14*, 1−12.
(25) Chou, J. J.; Bax, A. *J. Am. Chem. Soc.* **2001**, *123*, 3844−3845.
(26) Mittermaier, A.; Kay, L. E. *J. Am. Chem. Soc.* **2001**, *123*, 6892−6903.
(27) Lam, P. Y. S.; Jadhav, P. K.; Eyermann, C. J.; Hodge, C. N.; Ru, Y.; Bacheler, L. T.; Meek, J. L.; Otto, M. J.; Rayner, M. M.; Wong, Y. N.; Chang, C. H.; Weber, P. C.; Jackson, D. A.; Sharpe, T. R.; Ericksonviitanen, S. *Science* **1994**, *263*, 380−384.
(28) Yamazaki, T.; Nicholson, L. K.; Torchia, D. A.; Stahl, S. J.; Kaufman, J. D.; Wingfield, P. T.; Domaille, P. J.; Campbellburk, S. *Eur. J. Biochem.* **1994**, *219*, 707−712.
(29) Ruckert, M.; Otting, G. *J. Am. Chem. Soc.* **2000**, *122*, 7793−7797.
(30) Hansen, M. R.; Mueller, L.; Pardi, A. *Nat. Struct. Biol.* **1998**, *5*, 1065−1074.
(31) Delaglio, F.; Grzesiek, S.; Vuister, G. W.; Zhu, G.; Pfeifer, J.; Bax, A. *J. Biomol. NMR* **1995**, *6*, 277−293.
(32) Wang, A. C.; Grzesiek, S.; Tschudin, R.; Lodi, P. J.; Bax, A. *J. Biomol. NMR* **1995**, *5*, 376−382.
(33) Grzesiek, S.; Bax, A. *J. Am. Chem. Soc.* **1992**, *114*, 6291−6293.
(34) Ottiger, M.; Delaglio, F.; Marquardt, J. L.; Tjandra, N.; Bax, A. *J. Magn. Reson.* **1998**, *134*, 365−369.

(SVD),[35,36] using the program PALES.[37] Proton positions were added to the GB3 crystal structure using XPLOR.[38]

DFT Calculations. DFT calculations were carried out on conformers of a valine and threonine dipeptide analogue, Ace-Val-Nme and Ace-Thr-Nme. The ϕ and ψ backbone angles were constrained to (−57,−47) for "helix" structures, and to (−120,120) for "sheet" structures. For each of these typical backbone torsion pairs, χ_1 values were varied on a 15° grid, with all remaining degrees of freedom optimized using Hartree−Fock theory and a 6-31G basis set. Indirect spin−spin coupling constants were determined using the deMon program.[39−41] We used the IGLO-III basis set of Kutzelnigg and co-workers;[42] this is a relatively large basis set, with 11 s-type and 7 p-type Gaussians on first row atoms (contracted to 7s/6p), along with two uncontracted polarization functions. All calculations used the Perdew exchange and correlation functionals,[43,44] as recommended for spin−spin coupling constants with this procedure.[40,41] The diamagnetic spin−orbit (DSO), paramagnetic spin−orbit (PSO), and Fermi contact (FC) contributions are computed with this approach. For the Fermi term, a finite perturbation approach is used, so that a separate calculation is needed for each nucleus, although such a calculation then gives couplings to all other nuclei in the molecule. The DSO and PSO terms are small and partially cancel, so that the net coupling is dominated by the FC term. For example, for the threonine dipeptide with $(\phi,\psi,\chi_1) = (-57,-47,-120)$, the FC, DSO, and PSO contributions to $^3J_{C'-C\gamma}$ are 2.01, 0.11, and −0.14 Hz, respectively. In all, 96 geometry optimizations and coupling constant calculations were carried out (2 sequences × 2 backbone conformations × 24 side-chain conformations). An additional 48 coupling constant calculations were performed for Val, to obtain couplings from both the $C^{\gamma 1}$ and the $C^{\gamma 2}$ atoms.

Results for all of the DFT calculations are given in the Supporting Information. As a check on the basis-set and functional dependence of the results, we repeated the coupling constant calculations for valine in the sheet backbone conformation, using the B3LYP functional and the 6-311G(2d,p) basis set. The results for the Cγ−C′ couplings were essentially indistinguishable from those described above, with maximum couplings differing by less than 0.1 Hz from the results reported here.

Results and Discussion

The aim of the present study is to derive approximate order parameters for Val, Thr, and Ile side chains in proteins from a simple measurement of $^3J_{NC\gamma}$ and $^3J_{C'C\gamma}$. A prerequisite for this approach is the accurate parametrization of the corresponding Karplus relations between χ_1 and the value of these couplings. Such parametrization is straightforward when the torsion angles are static and known accurately, but we find that in proteins many of the side chains are subject to rotameric averaging. Instead, the approach we have chosen for defining the applicable χ_1 angles determines the collection of rotamer ensembles compatible with side-chain dipolar couplings measured in two liquid crystalline media, assuming the backbone conformation remains identical to that in either the high resolution (1.1 Å) X-ray structure of GB3[45] or the NMR solution structure of ubiquitin.[46,47] Empirical Karplus parametrization then entails optimization of the fit between measured $^3J_{N-C\gamma}$ and $^3J_{C'-C\gamma}$ values and values predicted by the empirical Karplus equations, averaged over the corresponding ensemble derived from dipolar couplings. We first discuss the generation of rotamer ensembles, followed by the empirical Karplus parametrization, and determination of order parameters derived from the *J* couplings.

Determination of χ_1 Ensemble from Dipolar Couplings. The fit of dipolar couplings to multiple side-chain rotamers in proteins previously has been addressed by Mittermaier and Kay.[26] In the case of multiple side-chain conformers, they interpreted their data in terms of ideally staggered rotamers. With this assumption, we find that Karplus parameters derived from these ideally staggered rotamers, populated according to dipolar coupling information, yield nonoptimal cross-validation statistics. For example, when one uses Karplus parameters derived for GB3 to predict $^3J_{C'C\gamma}$ and $^3J_{NC'}$ in ubiquitin, using rotamer populations best-fit to dipolar couplings, considerably poorer agreement is obtained than in the case where deviations from ideal staggering are considered (Supporting Information). However, permitting arbitrary deviations from ideally staggered rotamers introduces so many degrees of freedom that the problem of determining their populations becomes underdetermined. Instead, we use a compromise where small (<30°) deviations are allowed and which appears to optimize cross-validation results. Measurement of dipolar couplings in multiple liquid crystalline media, yielding linearly independent dipolar coupling information,[36,47,48] is needed to permit introduction of these additional variables. For ubiquitin, dipolar couplings were measured previously, both in neutral and in charged bicelles;[49] for GB3, measurements were carried out in liquid crystalline Pf1 and PEG media. $C^{\gamma}H_3$ and $C^{\beta}H^{\beta}$ dipolar couplings of Val, Ile, and Thr residues were measured with the *J*-modulated [^{1}H−^{13}C] CT-HSQC experiment.[34] For a rapidly spinning C^{γ} methyl group, $^1D_{C\gamma-H3}$ is reduced relative to a static ^{13}C−^{1}H interaction in the $C^{\beta-}C^{\gamma}$ direction by a factor $P_2(\cos\theta)$, with $P_2(x) = (3x^2 - 1)/2$, and for a methyl group $\theta = 110.9°$.[50] The dipolar contribution to the $^1J_{CH}$ splitting therefore can be used directly to constrain the orientation of the C−CH_3 bond. When combining the data collected in two alignment media, a total of six dipolar couplings ($^1D_{C\gamma1-H3}$, $^1D_{C\gamma2-H3}$, and $^1D_{C\beta H\beta}$) for Val and four dipolar couplings ($^1D_{C\gamma2-H3}$ and $^1D_{C\beta-H\beta}$) for Ile and Thr residues are available to determine the χ_1 rotamer populations. Also obtained from the same experiment is a complete set of backbone $^1D_{C\alpha-H\alpha}$ dipolar couplings, which is used to define the alignment tensors by best-fitting these couplings to the known structure.[35,36] With a Pearson's correlation coefficient of $R_P = 0.99$, $^1D_{C\alpha-H\alpha}$ values measured for GB3 in PEG and Pf1 media fit very well to the 1.1 Å X-ray structure (PDB code 1IGD). Similar agreement was obtained when fitting ubiquitin $^1D_{C\alpha-H\alpha}$ couplings to its solution structure (PDB code 1D3Z),

(35) Losonczi, J. A.; Andrec, M.; Fischer, M. W. F.; Prestegard, J. H. *J. Magn. Reson.* **1999**, *138*, 334−342.
(36) Sass, J.; Cordier, F.; Hoffmann, A.; Cousin, A.; Omichinski, J. G.; Lowen, H.; Grzesiek, S. *J. Am. Chem. Soc.* **1999**, *121*, 2047−2055.
(37) Zweckstetter, M.; Bax, A. *J. Am. Chem. Soc.* **2000**, *122*, 3791−3792.
(38) Brunger, A. T. *XPLOR: A System for X-ray Crystallography and NMR*, 3.1 ed.; Yale University Press: New Haven, 1993.
(39) Malkina, O. L.; Salahub, D. R.; Malkin, V. G. *J. Chem. Phys.* **1996**, *105*, 8793−8800.
(40) Malkin, V. G.; Malkina, O. L.; Salahub, D. R. *Chem. Phys. Lett.* **1994**, *221*, 91−99.
(41) Malkin, V. G.; Malkino, O. L.; Eriksson, L. A.; Salahub, D. R. In *Modern density functional theory: A tool for chemistry*; Seminario, J. M., Politzer, P., Eds.; Elsevier: Leiden, 1995; pp 273−347.
(42) Kutzelnigg, W.; Fleischer, U.; Schindler, M. In *NMR, Basic Principles and Progress*; Diehl, P., Fluck, E., Gnther, H., Kosfeld, R., Seelig, J., Eds.; Springer: Berlin, 1990; Vol. 23, pp 167−262.
(43) Perdew, J. P. *Phys. Rev. B* **1986**, *33*, 8822−8824.
(44) Perdew, J. P.; Wang, Y. *Phys. Rev. B* **1992**, *45*, 13244−13249.
(45) Derrick, J. P.; Wigley, D. B. *J. Mol. Biol.* **1994**, *243*, 906−918.
(46) Cornilescu, G.; Marquardt, J. L.; Ottiger, M.; Bax, A. *J. Am. Chem. Soc.* **1998**, *120*, 6836−6837.
(47) Ramirez, B. E.; Bax, A. *J. Am. Chem. Soc.* **1998**, *120*, 9106−9107.
(48) Al-Hashimi, H. M.; Valafar, H.; Terrell, M.; Zartler, E. R.; Eidsness, M. K.; Prestegard, J. H. *J. Magn. Reson.* **2000**, *143*, 402−406.
(49) Ottiger, M.; Bax, A. *J. Am. Chem. Soc.* **1998**, *120*, 12334−12341.
(50) Ottiger, M.; Bax, A. *J. Am. Chem. Soc.* **1999**, *121*, 4690−4695.

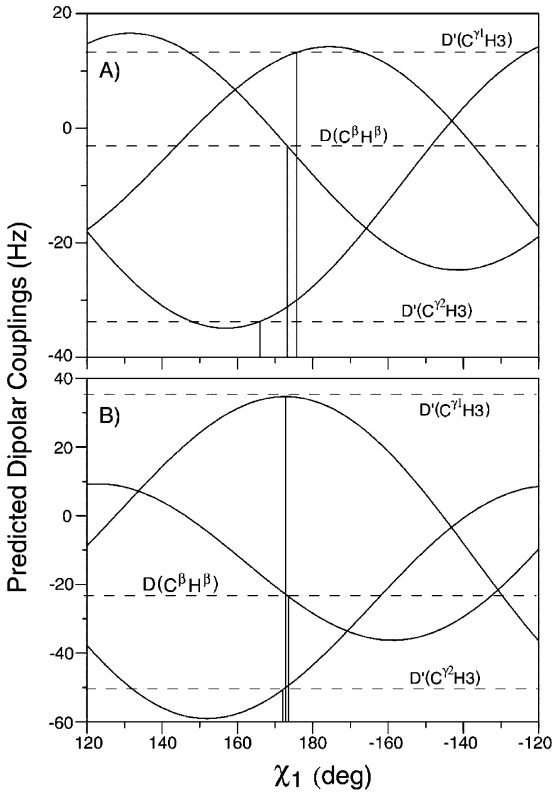

Figure 1. Calculated normalized dipolar couplings for $^1D_{C\beta-H\beta}$, $^1D_{C\gamma1-H3}$, and $^1D_{C\gamma2-H3}$ as a function of the χ_1 angle of Val[26] in ubiquitin, in (A) neutral bicelles and (B) charged bicelles. Values are calculated on the basis of the known backbone geometry (PDB code 1D3Z) and an alignment tensor derived from the $^1D_{C\alpha-H\alpha}$ values. Solid curves correspond to the calculated dipolar couplings; dashed lines are the experimental values. Vertical lines correspond to the intersect between measured values and the corresponding χ_1 dependent curve. $^1D_{C\gamma-H3}$ values have been normalized relative to $^1D_{C\beta-H\beta}$ by dividing the measured $^1D_{C\gamma-H3}$ value by $P_2(\cos 110.9°)$.

permitting the corresponding alignment tensors (Saupe matrixes) to be determined at high accuracy.

Knowledge of the precise Saupe matrix elements permits calculation of the side-chain $C_\beta-C_\gamma$ and $C_\beta-H_\beta$ dipolar couplings as a function of the χ_1 torsion angle. In the absence of internal mobility, there must be a χ_1 angle at which the observed and calculated $^1D_{C\gamma1-H3}$, $^1D_{C\gamma2-H3}$, and $^1D_{C\beta-H\beta}$ values agree within the margin of error in measurement and structure. Val[26] in ubiquitin is an example of such a case. This residue is located near the middle of an α-helix and exhibits large trans $^3J_{C'-C\gamma2}$ and $^3J_{N-C\gamma1}$ values of 4.18 and 2.16 Hz, respectively. Previously, a high order parameter ($S^2 = 0.93$) has been measured for this residue by ^{2}H relaxation.[51] As can be seen in Figure 1, its experimental $^1D_{C\gamma1-H3}$, $^1D_{C\gamma2-H3}$, and $^1D_{C\beta-H\beta}$ values intersect the predicted dipolar coupling curve at approximately the same torsion angle, $\chi_1 = 173 \pm 3°$. For most other residues, however, smaller trans J couplings are observed, and, at the same time, dipolar couplings are not simultaneously compatible with a single χ_1 angle. For these residues, a search is performed to find all distributions of the three staggered rotamers that yield a good match between calculated and observed dipolar couplings. In doing so, we assume jumps among three energetically favorable rotamers (χ_1 of 180, −60, and +60), each with an arbitrary twist angle, or deviation from the ideal rotamer, no greater than ±30°. Small scale harmonic oscillations around a given torsion angle are not taken into consideration as they only result in a slight reduction of the dipolar coupling magnitude. In this study, the three rotamer populations being searched are referred to as $P(180 + \omega^{180})$, $P(-60 + \omega^{-60})$, and $P(60 + \omega^{+60})$, which must sum to unity, and the allowed twist angles ω each fall in the range from −30° to +30°. The resolution of the resulting five-dimensional grid search (over two relative populations and the three ω angles) is 2% for the populations and 2° for the twist angles. In this grid search, the root-mean-square difference (rmsd) between measured dipolar couplings and those predicted on the basis of the three rotamer populations for the $C_\beta-C_\gamma$ and $C_\beta-H_\beta$ bond vectors is used to identify allowed rotamer combinations. All combinations that predict the dipolar coupling within experimental error are retained. This selection criterion therefore includes, without bias, all possible solutions, which subsequently are used for Karplus parameter optimization. The number of solutions in agreement with the dipolar coupling varies considerably among residues, depending on the orientation of the side chain relative to the two alignment tensor principal axes systems. Table 1 summarizes these rotamer populations and the corresponding average χ_1 angles, with their standard deviations for ubiquitin. Analogous data for GB3 are available as Supporting Information.

Parametrization of $^3J_{N-C\gamma}$ and $^3J_{C'-C\gamma}$ Karplus Relations. The full ensemble of allowed rotamers determined by dipolar couplings is used to parametrize the Karplus equation for $^3J_{N-C\gamma}$ and $^3J_{C'-C\gamma}$ couplings. The general form for the Karplus equation is

$$J(\phi) = A\cos^2(\phi + \delta) + B\cos(\phi + \delta) + C \qquad (1)$$

where ϕ is the applicable torsion angle, and δ is a small phase shift, which is found to deviate from zero, in particular, for Thr residues. Optimization of the Karplus curve parametrization involves the search for A, B, C, and δ values that yield optimal agreement between observed J values and $\langle^3J_{XY}\rangle$ calculated from eq 1, after averaging over all M solutions of the dipolar grid search, described above:

$$\langle^3J_{XY}\rangle = (1/M)\sum_{i=1,..,M}[P_i^{180}J(\phi_i^{180}) + P_i^{-60}J(\phi_i^{-60}) + P_i^{+60}J(\phi_i^{+60})] \qquad (2)$$

with X = N or C′, Y = $C^{\gamma1}$, $C^{\gamma2}$ for Val, and Y = $C^{\gamma2}$ for Ile and Thr, and P_i^r and ϕ_i^r are the population and the corresponding $X-C^\alpha-C^\beta-Y$ dihedral angle of each rotamer ($r = 180°$, −60°, and +60°) for solution i. Because of the nature of the quantitative J correlation method, used here for coupling measurement, the error in the J coupling scales approximately with the inverse of its magnitude.[22] To include this effect in the search, the difference between individual pairs of predicted and observed J couplings is weighted by the magnitude of the observed coupling. In addition, to account for the smaller range of $^3J_{NC\gamma}$ relative to $^3J_{C'C\gamma}$, a scaling factor, p, is introduced with $p = 1$ for $^3J_{C'-C\gamma}$, and $p = 2$ for $^3J_{N-C\gamma}$. The search for the optimal Karplus parameters then aims to minimize

$$Q = \{(1/k)\sum_{i=1,...,k}(J_{XY,i}^{obs})^2[p\langle^3J_{XY,i}\rangle - pJ_{XY,i}^{obs}]^2\}^{1/2} \qquad (3)$$

(51) Lee, A. L.; Flynn, P. F.; Wand, A. J. *J. Am. Chem. Soc.* **1999**, *121*, 2891−2902.

Table 1. Side-Chain Rotamer Populations (P) and Corresponding Average χ_1 Angles of Val, Ile, and Thr Residues in Ubiquitin[a]

residue	P^{180}	P^{-60}	P^{+60}	χ_1^{180}	χ_1^{-60}	χ_1^{+60}	χ_1 (X-ray)[b]
V5	0.92 (0.03)	0.06 (0.02)	0.02 (0.02)	182 (3)	−61 (18)	59 (18)	180
V17	0.04 (0.03)	0.96 (0.03)	0.00 (0.00)	178 (17)	−68 (4)	60 (18)	−63
V26	1.00 (0.01)	0.00 (0.00)	0.00 (0.01)	173 (1)	−60 (18)	58 (18)	168
V70	0.36 (0.11)	0.59 (0.10)	0.05 (0.05)	191 (9)	−46 (8)	58 (18)	177
I3	0.21 (0.20)	0.32 (0.17)	0.47 (0.18)	184 (19)	−80 (10)	59 (14)	60
I13	0.01 (0.01)	0.75 (0.01)	0.24 (0.02)	181 (18)	−54 (3)	57 (7)	126
I23	0.07 (0.06)	0.89 (0.04)	0.04 (0.04)	190 (17)	−69 (2)	50 (18)	−61
I30	0.01 (0.02)	0.99 (0.02)	0.00 (0.01)	176 (19)	−70 (1)	60 (18)	−71
I36	0.10 (0.04)	0.90 (0.04)	0.00 (0.00)	158 (6)	−61 (4)	60 (18)	−54
I44	0.06 (0.02)	0.91 (0.01)	0.03 (0.01)	177 (18)	−66 (4)	62 (18)	−49
I61	0.01 (0.01)	0.98 (0.02)	0.01 (0.01)	181 (18)	−73 (4)	60 (18)	−70
T7	0.05 (0.03)	0.12 (0.08)	0.83 (0.07)	180 (18)	−68 (17)	59 (7)	77
T9	0.01 (0.02)	0.20 (0.07)	0.79 (0.09)	181 (18)	−83 (5)	57 (5)	71
T12	0.01 (0.01)	0.89 (0.01)	0.10 (0.02)	177 (18)	−64 (1)	76 (9)	−63
T14	0.03 (0.02)	0.83 (0.01)	0.14 (0.02)	182 (18)	−63 (3)	53 (15)	67
T22	0.11 (0.01)	0.00 (0.01)	0.89 (0.02)	163 (9)	−60 (18)	57 (1)	61
T55	0.02 (0.02)	0.00 (0.00)	0.98 (0.02)	178 (18)	−60 (18)	61 (3)	60

[a] Values, derived from side-chain dipolar couplings in two liquid crystalline media, represent the mean of all possible solutions from the dipolar grid search; standard deviations are shown in parentheses. [b] The X-ray χ_1 angles are taken from the 1.8-Å X-ray structure of ubiquitin (PDB code 1UBQ).[53]

Table 2. Karplus Coefficients for $^3J_{N-C\gamma}$ and $^3J_{C'-C\gamma}$ in Val, Ile, and Thr[a]

	residue type	A	B	C	δ
		Best-Fit			
$^3J_{N-C\gamma 2}$	Thr	2.01	0.21	−0.12	7
$^3J_{N-C\gamma}$	Val, Ile	2.64	0.26	−0.22	6
$^3J_{C'-C\gamma 2}$	Thr	2.76	−0.67	0.19	17
$^3J_{C'-C\gamma}$	Val, Ile	3.42	−0.59	0.17	5
		DFT[b]			
$^3J_{N-C\gamma 2}$	Thr	2.12	0.23	−0.15	13
$^3J_{N-C\gamma 1}$	Val	2.22	0.15	−0.06	3
$^3J_{N-C\gamma 2}$	Val	2.24	0.15	−0.03	−9
$^3J_{C'-C\gamma 2}$	Thr	2.97	−0.83	−0.02	25
$^3J_{C'-C\gamma 1}$	Val	3.31	−0.91	0.01	16
$^3J_{C'-C\gamma 2}$	Val	3.30	−0.51	0.04	4

[a] Parameters for the generalized Karplus expression (eq 1). [b] DFT coefficients are the averages of fits for the helix and sheet backbone conformations.

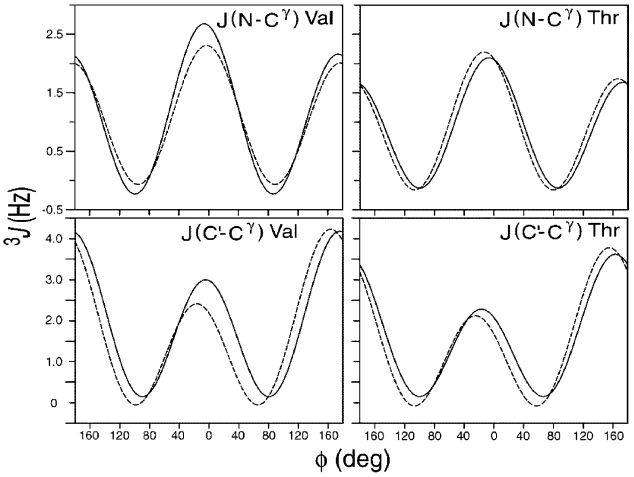

Figure 2. Karplus curves parametrized with experimental J couplings (solid) and those derived by best-fitting the results of DFT calculations (dashed), using the parameters of Table 2. For valine, the curves show the best fit to the combined data for Cγ1 and Cγ2. The ϕ angle is defined in eq 1.

where the summation extends over all k $^3J_{N-C\gamma}$ and $^3J_{C'-C\gamma}$ couplings of residues for which rotamer populations were derived from dipolar couplings, and for which experimental couplings, J_{XY}^{obs}, were obtained. In this process, couplings measured for Val and Ile residues in GB3 and ubiquitin were pooled together in the summation of eq 3 because their very similar covalent structure is likely to result in negligible differences in their Karplus parametrizations. However, Thr residues were treated separately because both experimental data (Supporting Information Table 2) and calculations indicate that its trans J values are considerably smaller than those in Val and Ile residues.

The minimization of Q in eq 3 is carried out using a Monte Carlo minimization procedure, which was found to be stable provided reasonable starting values were used for the Karplus parameters. The fitting routine for Val and Ile converges at $Q = 0.39$ Hz^2, and the root-mean-square difference (rmsd) between predicted and measured couplings is 0.25 Hz, whereas for Thr, $Q = 0.32$ Hz^2 and rmsd $= 0.21$ Hz. The resulting optimized Karplus coefficients for Val/Ile and Thr are presented in Table 2. The maxima of these Karplus curves correspond to values of 2.16 and 4.18 Hz for $^3J_{N-C\gamma}$ and $^3J_{C'-C\gamma}$ in Val and Ile residues, respectively, which are very close to the largest observed values (Supporting Information). The maximum predicted couplings for Thr are considerably smaller, 1.68 and 3.62 Hz, while the maximum observed values are slightly smaller (1.61 and 3.39 Hz).

Comparison of Computational and Empirical Karplus Parametrization. Figure 2 and Table 2 compare the empirically parametrized Karplus relations with those obtained from DFT calculations. Because differences between the DFT coefficients for the helix and sheet backbone conformers were small, only the average coefficients are reported. For Val and Ile residues, the simulated and experimental curves agree quite well, except for the eclipsed orientation, where the dihedral angle is near zero. This latter discrepancy is not surprising as there are essentially no experimental data in this region. The agreement between simulated and experimental curves is even better for Thr, despite the occurrence of a relatively large and unusual phase shift, δ, of about 25° in the $^3J_{C'-C\gamma}$ Karplus curve derived by DFT. The experimentally parametrized $^3J_{C'-C\gamma}$ curve also shows a large positive phase shift of 17°, in remarkable agreement with the DFT results. The DFT and fit results for Thr also agree in giving a phase shift for $^3J_{N-C\gamma}$ that is about 10° smaller than that for $^3J_{C'-C\gamma}$.

The situation is somewhat more complex for Val, because the DFT simulations show somewhat different behavior for $C^{\gamma 1}$ as compared to $C^{\gamma 2}$. For both the C−C and the C−N couplings, the DFT results indicate that the $C^{\gamma 2}$ phase shift is about 12° smaller than that for $C_{\gamma 1}$ (see Table 2). (Because of the way side-chain atoms are defined in the IUPAC nomenclature, the $C^{\gamma 2}$ group of Thr occupies a position analogous to that of the $C^{\gamma 1}$ group in Val.) The fitted parameters assume identical Karplus curves for both methyl groups of Val, which may affect a quantitative comparison of fitted and DFT results. At a qualitative level, however, both the fitted and the DFT results agree that the phase shifts for Val are less positive than those for Thr, for both C−C and C−N couplings; there is also agreement that the trans couplings for both C−C and C−N should be larger in Val than in Thr residues. Moreover, both the calculated and the experimental $^3J_{N-C\gamma}$ curves show a positive value for the Karplus constant, *B*, resulting in a cis value for this type of coupling that is larger than the trans value.

Order Parameters from ^3J Couplings. Using the Karplus parameters of Table 2, we wish to evaluate how well the χ_1 rotamer distribution is defined by the experimental $^3J_{N-C\gamma}$ and $^3J_{C'-C\gamma}$ values. The search routine described above for fitting the rotamer populations to dipolar couplings is adapted for defining all rotamers compatible with the experimental ^3J couplings. Here, the Karplus equations are used to calculate the couplings at any given χ_1 angle, and the search objective is to find the rotamer distributions that yield the lowest rmsd's between observed and calculated $^3J_{N-C\gamma}$ and $^3J_{C'-C\gamma}$. In analogy to eq 3, the function to be minimized is given by

$$Q = \{(1/n) \sum_{i=1,..,n} [(J_i^{obs})^2 (pJ_i^{calc} - pJ_i^{obs})^2]\}^{1/2} \qquad (4)$$

where the summation extends over all *n* couplings measured for a given residue and used in the search, typically $n = 4$ for Val ($^3J_{C'-C\gamma 1}$,$^3J_{C'-C\gamma 2}$, $^3J_{N-C\gamma 1}$, and $^3J_{N-C\gamma 2}$), and $n = 2$ for Ile and Thr.

The aim of the *J* coupling analysis is to determine for each residue two independent rotamer populations and three independent twist angles (≤30°), which describe deviations from ideally staggered rotamers. Clearly, with only two measured couplings for Thr and Ile residues (four for Val), this problem is underdetermined, and an ensemble of solutions is obtained.

For each member of the ensemble of solutions, a generalized order parameter, $\boldsymbol{S}_J^2$, can be calculated from the *J*-coupling-derived rotamer combinations:

$$\boldsymbol{S}_J^2 = \sum_{i,j} P_i P_j (3 \cos^2 \theta_{ij} - 1)/2; \quad i = 1,2,3; j = 1,2,3 \qquad (5)$$

where the summation extends over all pairwise combinations of the three rotamers, P_i is the population of rotamer *i*, and θ_{ij} is the angle between the $C_\beta-C_\gamma$ bond vectors of rotamers *i* and *j*.

The $^3J_{N-C\gamma}$ and $^3J_{C'-C\gamma}$ values, measured for Val, Ile, and Thr residues in ubiquitin and HIV-protease, were converted into rotamer populations in the above-described manner. For each solution, an order parameter $\boldsymbol{S}_J^2$ is calculated from eq 5 (Table 3). As pointed out above, the number of *J* couplings available per residue generally is insufficient to define uniquely the set of applicable rotamers. Therefore, $\boldsymbol{S}_J^2$ values are calculated for each of the solutions to eq 4, and the mean, the standard deviation, and the entire range of the $\boldsymbol{S}_J^2$ ensemble are retained.

Table 3. Generalized Order Parameters Derived from Experimental $^3J_{N-C\gamma}$ and $^3J_{C'-C\gamma}$ ($\boldsymbol{S}_J^2$), Dipolar Couplings ($\boldsymbol{S}_D^2$), and ^{2}H Relaxation Rates ($\boldsymbol{S}_{rel}^2$) in Ubiquitin[a]

γ-carbon	$\boldsymbol{S}_J^2$ mean	$\boldsymbol{S}_J^2$ min–max	$\boldsymbol{S}_D^2$ mean	$\boldsymbol{S}_D^2$ min–max	$\boldsymbol{S}_{rel}^2$ [b]
V5γ	0.70	0.64−0.81	0.80	0.65−0.90	0.89
V17γ	0.83	0.76−0.90	0.91	0.78−1.00	0.89
V26γ	0.99	0.96−1.00	1.00	0.95−1.00	0.92
V70γ	0.31	0.20−0.53	0.36	0.26−0.55	0.35
I3γ2	0.71	0.65−0.81	0.38	0.21−0.85	0.98
I13γ2	0.25	0.14−0.59	0.46	0.40−0.52	0.56
I23γ2	0.88	0.56−1.00	0.69	0.52−0.84	0.95
I30γ2	0.86	0.53−1.00	0.98	0.87−1.00	0.93
I36γ2	0.86	0.56−0.96	0.82	0.72−0.93	0.83
I44γ2	0.43	0.28−0.68	0.79	0.68−0.91	0.71
I61γ2	0.90	0.66−1.00	0.95	0.88−1.00	0.95
T7γ2	0.62	0.51−0.75	0.65	0.50−0.84	0.75
T9γ2	0.72	0.63−0.83	0.66	0.42−0.90	0.64
T12γ2	0.79	0.40−1.00	0.79	0.72−0.87	0.93
T14γ2	0.58	0.30−1.00	0.61	0.56−0.66	0.78
T22γ2	0.97	0.91−1.00	0.72	0.64−0.78	0.95
T55γ2	0.74	0.64−0.85	0.95	0.83−1.00	0.93

[a] The mean $\boldsymbol{S}^2$ values of solution ensembles, derived from ^3J and dipolar couplings, are shown, respectively, in columns 2 and 4; columns 3 and 5 present the full $\boldsymbol{S}^2$ ranges. [b] Values reported by Lee et al.,[51] derived from ^{2}H relaxation rates.

Figure 3A compares the $\boldsymbol{S}_J^2$ with the $\boldsymbol{S}_{rel}^2$ values, previously extracted from methyl ^{2}H relaxation rates for the two proteins. With a correlation coefficient of 0.81, the correlation between $\langle \boldsymbol{S}_J^2 \rangle$ and $\boldsymbol{S}_{rel}^2$ is remarkably good, particularly considering that $\boldsymbol{S}_J^2$ and $\boldsymbol{S}_{rel}^2$ measure the order parameter on very different time scales. The ^{2}H relaxation derived $\boldsymbol{S}_{rel}^2$ values relate to order on a time scale faster than the overall rotational correlation time of the protein. $\boldsymbol{S}_J^2$ values describe order on a millisecond time scale. The lower values of $\boldsymbol{S}_J^2$ relative to $\boldsymbol{S}_{rel}^2$ therefore may result from motions on a time scale slower than the overall rotational tumbling. However, for many residues, the total range of $\boldsymbol{S}_J^2$ values that are compatible with a given *J* coupling is relatively large due to the above-mentioned underdetermination of the rotamer populations, and the possibility that the lack of experimental observables causes $\boldsymbol{S}_J^2$ to be smaller than $\boldsymbol{S}_{rel}^2$ cannot be excluded.

To investigate whether the lower values of $\boldsymbol{S}_J^2$ are caused by slow internal motions or by the above sampling problem, we also calculate the order parameter derived from the dipolar coupling measurements. Up to six dipolar couplings are available (in two media) for Val, and four for Ile and Thr residues, so the rotamer ensemble is less underdetermined. Fully analogous to the $\boldsymbol{S}_J^2$ case, eq 5 can be used to derive $\boldsymbol{S}_D^2$ values from the ensemble of rotamers compatible with the experimental dipolar couplings (Supporting Information). For the vast majority of residues, the experimentally permissible ranges for $\boldsymbol{S}_J^2$ and $\boldsymbol{S}_D^2$ overlap, yielding an allowed range for the combined order parameter $\boldsymbol{S}_{J,D}^2$ that is smaller than that for $\boldsymbol{S}_J^2$ and $\boldsymbol{S}_D^2$ individually. For ubiquitin, both experimental ^{2}H relaxation-derived order parameters as well as *J* and dipolar couplings are available. Figure 3c shows that the correlation between $\boldsymbol{S}_{J,D}^2$ and $\boldsymbol{S}_{rel}^2$ is considerably better than that between $\boldsymbol{S}_J^2$ and $\boldsymbol{S}_{rel}^2$. Nevertheless, for several residues, notably Ile3, Val5, Thr12, Ile13, Thr14, and Ile23, $\boldsymbol{S}_{J,D}^2$ remains considerably smaller than $\boldsymbol{S}_{rel}^2$, indicating that rotameric averaging on a time scale slower than the rotational correlation time (4 ns) is taking

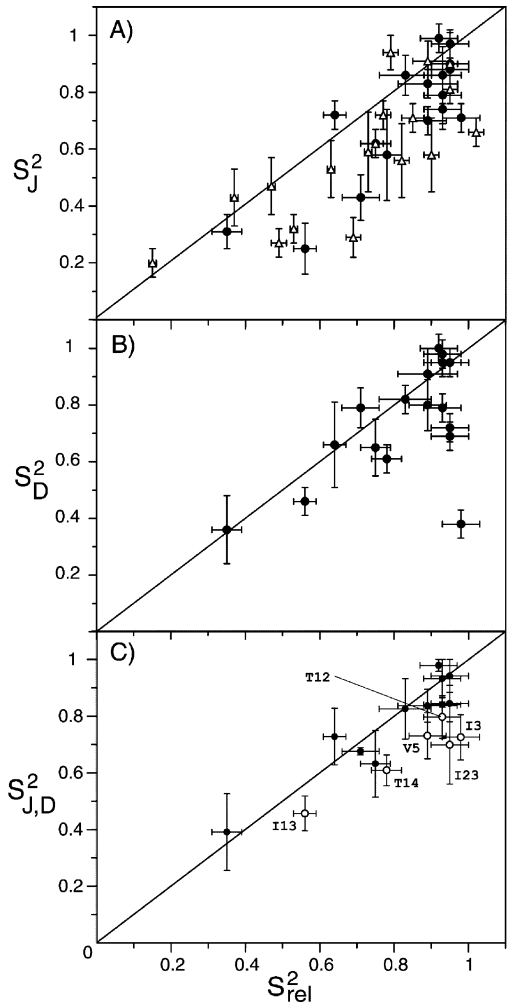

Figure 3. Methyl carbon generalized order parameters derived from (A) $^3J_{N-C\gamma}$ and $^3J_{C'-C\gamma}$ couplings (△, HIV protease; ●, ubiquitin), (B) dipolar couplings (ubiquitin only), and (C) combined *J* and dipolar couplings (ubiquitin only), versus corresponding literature values, $\boldsymbol{S}_{rel}^2$, derived from ^{2}H relaxation.[12,51] Vertical error bars in (A) and (B) correspond to the standard errors. Vertical error bars in (C) delimit overlap in the full ranges defined by the dipolar coupling and *J* coupling rotamer searches. Horizontal error bars correspond to previously reported uncertainties in $\boldsymbol{S}_{rel}^2$. Open symbols in (C) correspond to residues for which side-chain motion on a time scale slower than the overall tumbling of the molecule contributes to $\boldsymbol{S}_{J,D}^2$.

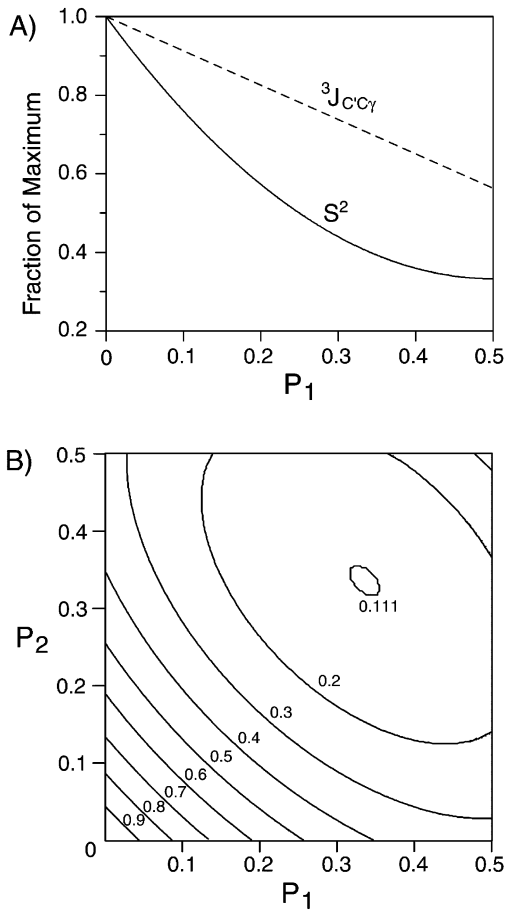

Figure 4. Dependence of $C^\beta-C^\gamma$ $\boldsymbol{S}^2$ on χ_1 rotamer distribution. (A) Relation between the population of the predominant rotamer (P_1) and $\boldsymbol{S}^2$ (solid curve). For comparison, the fractional decrease in $^3J_{C'-C\gamma}$ is also shown (dashed line). (B) Contour plot of the relation between $\boldsymbol{S}^2$ and populations of ideal $\chi_1 = -60°$, 60°, and 180° rotameric states.

place. The first five of these residues cluster together and are part of the first pair of ubiquitin's antiparallel β-strands. We speculate that the local stability of these secondary structure elements may be responsible for the high energetic barriers between side-chain χ_1 rotamers, resulting in the slow rates of rotameric averaging. Outside regions of secondary structure, there are no discrepancies exceeding the experimental uncertainty between the range of $\boldsymbol{S}_{J,D}^2$ values for ubiquitin, or $\boldsymbol{S}_J^2$ in HIV protease, and ^{2}H-derived $\boldsymbol{S}_{rel}^2$ order parameters.

It is interesting to note that eq 5 results in a considerable drop in $\boldsymbol{S}_J^2$ for relatively small populations of the minor conformers. This effect is illustrated in Figure 4, which demonstrates the calculated steep dependence of $\boldsymbol{S}_{rel}^2$ on the population of minor rotamers.

Concluding Remarks

Analysis of ^3J couplings in terms of populations of staggered rotamers has a rich history in NMR.[19−21] However, most of such analyses relied on the simplified assumption of ideal, 180°, or ±60° rotamers. Analysis of the $^3J_{N-C\gamma}$ and $^3J_{C'-C\gamma}$ couplings in our study is found to be incompatible with this assumption. For example, for Val[26] in ubiquitin, only a slightly twisted $\chi_1 = 172°$ rotamer fits the dipolar coupling data, and for this and numerous other residues there is no combination of ideally staggered rotamers that adequately fits the dipolar couplings. Considerable deviations from ideal staggering, with a standard deviation exceeding 10°, are also seen in atomic resolution crystal structures. Other evidence for the need to invoke deviations from the ideally staggered rotamers is found in cross validation: $^3J_{C'-C\gamma}$ and $^3J_{N-C\gamma}$ Karplus curves derived using dipolar and *J* coupling data from GB3 provide a considerably worse prediction for *J* values observed in ubiquitin when using ideally staggered rotamers than when using the "ensemble of skewed rotamers" approach (Supporting Information Table 4). The same applies when using ubiquitin data to predict GB3 *J* values. Indeed, it is reasonable to expect that, in particular, the lowly populated rotameric states, which are of higher energy, can deviate significantly from the perfectly staggered conformation. In this respect, it is also interesting to note that, for more than 85% of the side chains considered in GB3 and ubiquitin, the most highly populated rotamer agrees with the one observed by X-ray crystallography, and of these 28 residues, 25 are skewed in the same direction from ideal staggering as in the X-ray.

Up to nine ^3J couplings are, in principle, available to characterize the χ_1 angle in $^{13}C/^{15}N$ labeled proteins, and a variety of three-dimensional NMR experiments has been proposed to measure these couplings.[18] For Ile, Val, and Thr residues, the $^3J_{N-C\gamma}$ and $^3J_{C'-C\gamma}$ couplings are the most attractive of these because they can be measured at high accuracy from simple and sensitive two-dimensional experiments. However, with recent residue-specific parametrizations for the couplings in other types of residues,[18] side-chain rotamer populations are intrinsically accessible for all types of residues.

Parametrization of the Karplus equations for $^3J_{N-C\gamma}$ and $^3J_{C'-C\gamma}$ resulted in an unusual phase shift term (eq 1), both when using the results of the DFT calculations and when analyzing the experimental data. This phase shift is largest for Thr, but smaller phase shifts are also noticeable for Val and Ile. For Val and Ile, these phase shifts are likely to result from the chirality at the C^α site, because separate experimental parametrizations for the $^3J_{N-C\gamma1}$, $^3J_{N-C\gamma2}$, $^3J_{C'-C\gamma1}$, and $^3J_{C'-C\gamma2}$ Karplus curves result in comparably small positive phase shifts ($5 \pm 2°$) for all four curves (data not shown). For Thr, the larger phase shift presumably results from a combined effect of chirality at both the C^α and the C^β sites. The DFT results are similar, but for Val they also show phase shifts that are about 12° different for $C^{\gamma1}$ as compared to $C^{\gamma2}$.

Comparison of rotamer populations and the corresponding order parameter, $\boldsymbol{S}_J^2$, indicates that even low populations of minor conformers can result in a significant drop in $\boldsymbol{S}_J^2$. For example, if the major conformer is 80% populated, and both minor conformers are 10% occupied, $\boldsymbol{S}_J^2 = 0.55$ (see Figure 4). Intuitively, 80% population of the major conformer indicates a reasonably well-ordered system. However, when protein backbone order parameters are analyzed (usually on the basis of ^{15}N relaxation data), an $\boldsymbol{S}^2 = 0.55$ value suggests significant disorder, typically associated with highly mobile loop regions. The reason for this discrepancy lies in the different motional processes underlying the disorder. Backbone amide groups frequently are assumed to undergo oscillations about an average orientation, and substantial amplitudes in such a model are needed to reduce the order parameter significantly. For the side chains, the motional process is based on rotameric jumps. The large amplitude of such jumps, that is, the small value of $P_2(\mu_1 \cdot \mu_2)$ (where μ_1 and μ_2 represent $C^\beta - C^\gamma$ unit vectors in the two conformers), results in a substantial reduction in order parameter at relatively low population of the minor conformer. The lack of knowledge on the motional model underlying the $\boldsymbol{S}^2$ data derived from relaxation measurements interferes with a quantitative assessment of the entropy associated with such disorder. However, recently it has also been pointed out that if the motional model does not change upon complex formation, calculated changes in entropy are much more robust.[52]

The ^3J analysis introduced in this paper may be used as a simple and fast method for estimating the approximate side-chain rotamer distributions of Ile, Val, and Thr residues in proteins. These data complement dynamic information derived from ^2H relaxation measurements and can provide insight into motional processes taking place on time scales slower than the overall rotational correlation time.

Acknowledgment. We wish to thank Attila Szabo, Dennis A. Torchia, and Rieko Ishima for stimulating discussions and providing us with the HIV protease sample, and Ben Ramirez for the GB3 samples and the GB3 backbone assignments. J.J.C. is a GlaxoSmithKline Fellow of the Life Sciences Research Foundation. This work was partially supported by NIH grant GM45811 (to D.A.C.).

Supporting Information Available: Discussion of selection of rotamer model; one table with side-chain rotamer populations in ubiquitin and GB3 assuming ideally staggered rotamers; one table with values of $J(-60)$, $J(60)$, and $J(180)$ optimized for the ideally staggered rotamer model; one table with Karplus parameters optimized on different subsets of residues; one table comparing cross-validated agreement between observed and predicted J couplings for the skewed and ideal rotamer models; one table with the experimental $^3J_{C'-N}$ and $^3J_{C'-C\gamma}$ couplings for Val, Ile, and Thr residues in GB3, ubiquitin, and HIV protease; one table summarizing the rotamer populations and the corresponding average χ_1 angles, with their standard deviations and full range, as derived from dipolar couplings in two alignment media for GB3; one table listing the $\boldsymbol{S}_J^2$ and $\boldsymbol{S}_D^2$ values, together with literature $\boldsymbol{S}^2$ values, derived from ^2H relaxation, for C^γ methyl groups in GB3, and HIV protease; one table with the DFT results; one figure comparing the full range of $\boldsymbol{S}_D^2$ solutions in ubiquitin with literature $\boldsymbol{S}^2$ values derived from ^2H relaxation in ubiquitin; one figure comparing the full range of $\boldsymbol{S}_J^2$ solution in ubiquitin and HIV protease with literature $\boldsymbol{S}^2$ values derived from ^2H relaxation (PDF). This material is available free of charge via the Internet at http://pubs.acs.org.

JA029972S

(52) Prabhu, N. V.; Lee, A. L.; Wand, A. J.; Sharp, K. A. *Biochemistry* **2003**, *42*, 562−570.
(53) Vijay-Kumar, S.; Bugg, C. E.; Cook, W. J. *J. Mol. Biol.* **1987**, *194*, 531−544.